

## Article

# Estimating Above-Ground Biomass from Land Surface Temperature and Evapotranspiration Data at the Temperate Forests of Durango, Mexico

Marcela Rosas-Chavoya <sup>1</sup>, Pablito Marcelo López-Serrano <sup>2,\*</sup>, Daniel José Vega-Nieva <sup>3</sup>, José Ciro Hernández-Díaz <sup>2</sup>, Christian Wehenkel <sup>2</sup> and José Javier Corral-Rivas <sup>3</sup>

<sup>1</sup> Programa Institucional de Doctorado en Ciencias Agropecuarias y Forestales, Universidad Juárez del Estado de Durango, Durango 34239, Mexico

<sup>2</sup> Instituto de Silvicultura e Industria de la Madera, Universidad Juárez del Estado de Durango, Durango 34239, Mexico

<sup>3</sup> Facultad de Ciencias Forestales y Ambientales, Universidad Juárez del Estado de Durango, Durango 34239, Mexico

\* Correspondence: pmslopez@gmail.com; Tel.: +52-618-233-66-12

**Abstract:** The study of above-ground biomass (AGB) is important for monitoring the dynamics of the carbon cycle in forest ecosystems. The emergence of remote sensing has made it possible to analyze vegetation using land surface temperature (LST), Vegetation Temperature Condition Index (VTCI) and evapotranspiration (ET) information. However, relatively few studies have evaluated the ability of these variables to estimate AGB in temperate forests. The aim of the present study was to evaluate the relationship of LST, VTCI and ET with AGB in temperate forests of Durango, Mexico, regarding each season of the year and to develop a AGB estimation model using as predictors LST, VTCI and ET, together with topographic, reflectance and Gray-Level Co-Occurrence Matrix (GLCM) texture variables. A semi-parametric model was generated to analyze the linear and non-linear responses of the predictive variables of AGB using a generalized linear model (GAM). The results show that the best predictors of AGB were longitude, latitude, spring LST, ET, elevation VTCI, NDVI (Normalized Difference Vegetation Index), slope and GLCM mean ( $R^2 = 0.61$ ; RMSE = 28.33 Mg ha $^{-1}$ ). The developed GAM model was evaluated with an independent dataset ( $R^2 = 0.58$ ; RMSE = 31.21 Mg ha $^{-1}$ ), suggesting the potential of this modeling approach to predict AGB for the analyzed temperate forest ecosystems.

**Keywords:** AGB; surface temperature; Vegetation Temperature Condition Index; evapotranspiration



**Citation:** Rosas-Chavoya, M.; López-Serrano, P.M.; Vega-Nieva, D.J.; Hernández-Díaz, J.C.; Wehenkel, C.; Corral-Rivas, J.J. Estimating Above-Ground Biomass from Land Surface Temperature and Evapotranspiration Data at the Temperate Forests of Durango, Mexico. *Forests* **2023**, *14*, 299. <https://doi.org/10.3390/f14020299>

Academic Editor: Dmitry Schepaschenko

Received: 5 January 2023

Revised: 24 January 2023

Accepted: 1 February 2023

Published: 3 February 2023



**Copyright:** © 2023 by the authors. Licensee MDPI, Basel, Switzerland. This article is an open access article distributed under the terms and conditions of the Creative Commons Attribution (CC BY) license (<https://creativecommons.org/licenses/by/4.0/>).

## 1. Introduction

The study of forest biomass is crucial for monitoring the carbon dynamics of terrestrial ecosystems, which are relevant data in the climate change context [1]. Biomass estimation and monitoring allow the reserves and carbon capture rates of forest ecosystems to be quantified [2]. According to the Intergovernmental Panel on Climate Change (IPCC) United Nation Programme, carbon reserves in forest ecosystems are mainly found in the following places: above-ground biomass (AGB), below ground biomass, forest litter layer, woody debris and organic matter in soil [3,4].

AGB accounts for about 70% of the forest biomass and constitutes 30% of the carbon reserves in terrestrial ecosystems [5]. AGB is a central criterion for programs seeking climate change solutions, such as Reducing Emissions from Reforestation and Forest Degradation (REDD+) United Nations Programme, and carbon trading [5–7]. Direct methods to estimate AGB are based on field measurements, sometimes requiring destructive methods to determine the biomass of each subject, as well as the amount of carbon in a sample of trees, and lastly, generating mathematical models or allometric equations, which allow

indirect estimation, i.e., from dasometric measurements [8]. These data are fundamental for monitoring forest resources; however, they are highly expensive and require significant human effort.

Given this problem, the use of satellite technologies has been proposed, specifically remote sensors for AGB's indirect estimation. These have several benefits, including: (1) cost reduction, (2) data generation in difficult access areas, (3) data capture on a regional scale, (4) availability of historical data with consistent characteristics (i.e., periodic sampling, same schedule, same area) and (5) data capture from spectral bands beyond the visible spectrum [9]. Combining in situ measurement data with satellite data allows spatial and temporal expansion of AGB in forest ecosystems [10].

Multispectral data allow for the estimation of vegetation indices, important variables for analyzing photosynthetic activity and forest canopy structure [11,12]. Several studies have tried to estimate AGB from this type of data [6,9,10,13–15]. For example, López-Serrano et al. [10] used Normalized difference vegetation index (NDVI), Soil-adjusted vegetation index (SAVI), texture metrics of Gray-Level Co-Occurrence Matrix (GLCM) and topographic and climatic data to estimate AGB with SVM in temperate forests.

In addition, the land surface temperature (LST) is a variable that can be estimated from satellite images, with thermal infrared band data, which provides spectral information on the energy exchange between solar radiation and the surface [16,17]. For example, Leeuwen et al. [17] evaluated the use of LST data to monitor deforestation processes in tropical forests in Brazil and concluded that LST data allow distinguishing between wooded and deforested areas, as well as quantifying deforestation.

One of the most important aspects of the LST-vegetation relationship are the seasonal changes [17]. Pongratz et al. [18] observed that the LST increases in areas with less forest cover, especially in dry seasons, compared to denser forests. A few studies have evaluated the use of LST for estimating AGB [19]. For example, Jiang et al. [1] evaluated the LST potential to improve AGB predictions in Chinese coniferous forests. They concluded that incorporating LST data into nonlinear models improves the AGB estimation efficiency. These studies are, nevertheless, still relatively scarce. For example, in the literature review of landsat LST applications for forest resources monitoring by Rosas-Chavoya et al. [19], only one out the 155 reviewed studies in the period 1995–2020 used LST to map forest biomass.

On the other hand, evapotranspiration (ET) is deemed as a variable closely related to carbon fluxes and biomass incorporation into forest ecosystems [20–22]. The Moderate Resolution Imaging Spectroradiometer (MODIS) instrument delivers the ET-8 day product, which provides data on 8-day accumulated evapotranspiration ( $\text{kg m}^{-2}$ ). In addition, one factor faced by forest ecosystems is drought stress, which occurs when potential evapotranspiration is greater than actual evapotranspiration [23]. The Vegetation Temperature Condition Index (VTCI) has been used as an indicator of drought and vegetation water stress [24]. Although these environmental factors are determining criteria for forest ecosystems, an evaluation of their efficiency for AGB estimation is required.

The relationship between environmental variables and AGB is usually complex, so an algorithm that captures these non-linear relationships between the dependent variable (AGB) and the predictor variables is required. Generalized Additive Models (GAMs) can describe complex relationships between AGB and environmental predictor variables. That is why they are deemed suitable for research in forest areas [25,26].

The aim of this paper herein was to evaluate the relationship of satellite information (LST, VTCI and ET, at different seasons) with AGB in temperate forests of Durango, Mexico. It is also aimed at generating a model in which LST and some associated variables, such as LST, VTCI and ET, together with topographic, reflectance and texture variables, for the estimation of observed AGB from field data from Permanent Forest and Soil Research Sites (SPIFyS) in temperate forests of Durango, Mexico. This was based on the following hypotheses: (1) The AGB relationship is different according to climatic conditions of each season of the year; (2) LST, VTCI and ET, together with topographic, reflectance and texture variables, could potentially be used as AGB predictors.

## 2. Materials and Methods

This study was conducted in temperate forests of the state of Durango, Mexico (Figure 1), which covers approximately 4.9 million hectares. These forests grow in the region named Sierra Madre Occidental; they show a wide tree diversity, predominating the *Pinus* and *Quercus*. Their elevation gradient goes from 363 and 3190 m. The climate is temperate humid with summer rains; average annual temperature ranges from 8.2 to 26.2 °C, while the average annual precipitation ranges from 443 to 1452 mm [27].

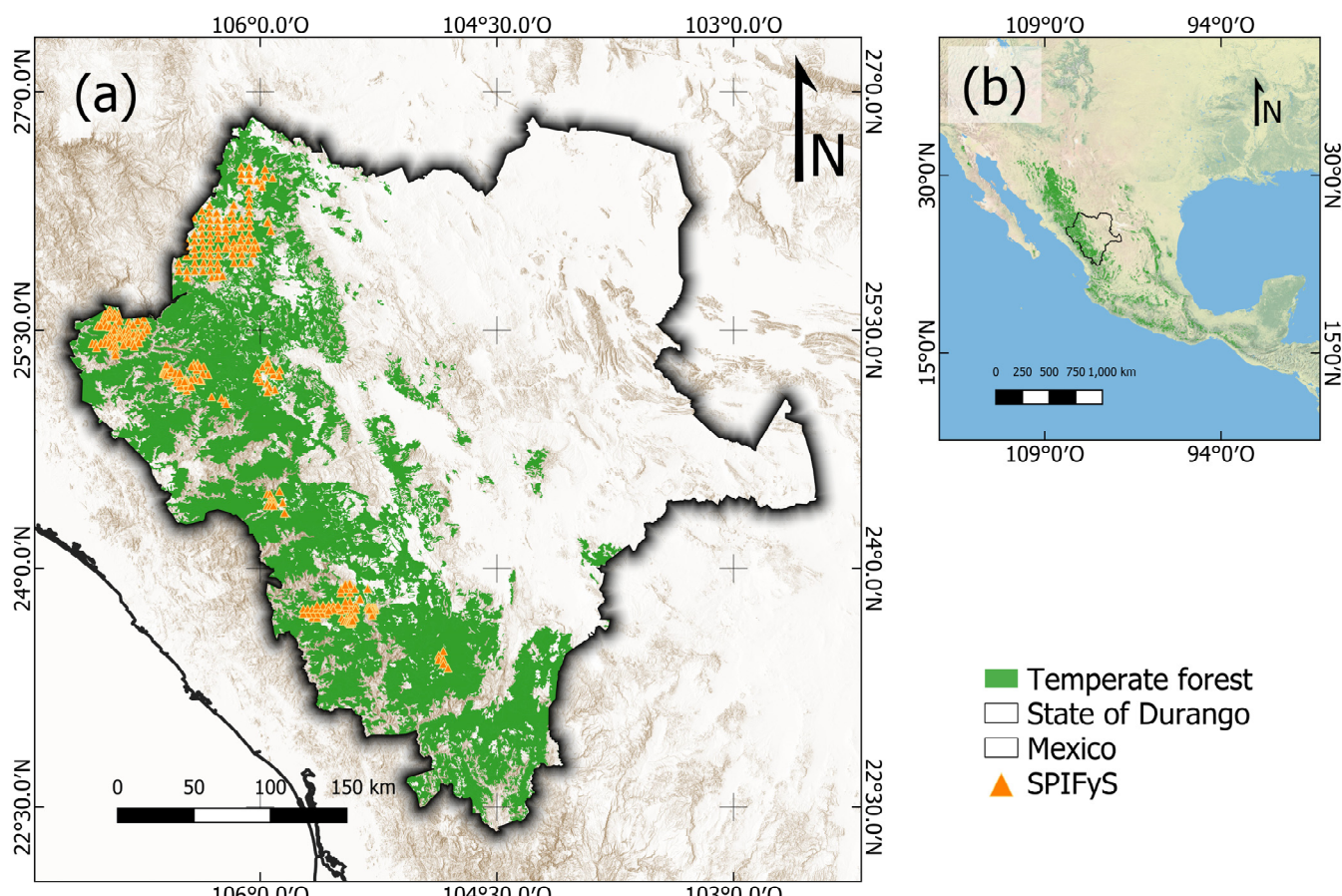


**Figure 1.** Study area. (a) Permanent forest and soil research sites (SPIFyS in Spanish). Temperate forest polygon taken from Land-Used Map Series VI, which was developed by the Instituto Nacional de Estadística y Geografía (INEGI). (b) Location of study area.

### 2.1. Field Data

The AGB field data correspond to 318 SPIFyS, which were settled in 2011 and have been sampled periodically (every 5 years). These are part of one of the most consistent databases on growth, production and evolution of forest stands in Mexico [28]. SPIFyS have a dimension of 50 × 50 m. At each plot, direct dasometric measurements were made, i.e., diameter at breast height, height and wood density. AGB ( $\text{Mg ha}^{-1}$ ) was subsequently calculated using allometric formulas previously developed by Vargas-Larreta et al. [29]. Data used in this study resulted from a sampling in winter 2017 (Table 1).

**Table 1.** Descriptive statistics of AGB field data from Durango temperate forests.

Plot Number	Range ( $\text{Mg ha}^{-1}$ )	Mean ( $\text{Mg ha}^{-1}$ )	Standard Deviation ( $\text{Mg ha}^{-1}$ )	Coefficient of Variation (%)
318	2.05–92.34	31.03	18.14	0.58

## 2.2. Image Acquisition

Landsat 8 satellite (OLI-TIRS) data were downloaded from the USGS Earth Resources Observation and Science (EROS) Center Science Processing Architecture (ESPA) platform, which allows requests for satellite products with different characteristics (i.e., radiometric correction, reference system, pixel size, file format) [30]. Bands 5 and 4 with SR correction were requested, and band 10 with brightness temperature data. Images from scenes 30/43, 30/44, 31/42, 31/43, 31/44, 32/42, 32/43 were selected for the four seasons of the year (Table 2). The selection criterion was the presence of less than 20% cloud cover.

**Table 2.** Path/Row and acquisition dates of utilized images for Landsat 8.

Row/Path	Acquisition Date			
	Winter	Spring	Summer	Autumn
30/43	4 February 2017	27 May 2017	30 July 2017	19 November 2017
30/44	4 February 2017	11 May 2017	30 July 2017	19 November 2017
31/42	11 February 2017	2 May 2017	22 August 2017	26 November 2017
31/43	11 February 2017	2 May 2017	22 August 2017	26 November 2017
31/44	11 February 2017	2 May 2017	6 August 2017	26 November 2017
32/42	2 February 2017	9 May 2017	29 August 2017	17 November 2017
32/43	2 February 2017	9 May 2017	29 August 2017	17 November 2017

Similarly, evapotranspiration data was obtained from the MODIS product “MODIS/Terra Net Evapotranspiration 8-Day V.6” [30], which has a resolution of 500 m and provides data on 8-day accumulated evapotranspiration ( $\text{kg m}^{-2}$ ) (Table 3).

**Table 3.** Path/Row and acquisition dates of utilized images for Evapotranspiration of MODIS.

Row/Path	Acquisition Start and End Dates			
	Winter	Spring	Summer	Autumn
MYD16A2 8/6	10 February 2017–17 February 2017	2017 May 17–2017 May 24	21 August 2017–28 August 2017	17 November 2017–24 November 2017

Lastly, a cloud and cloud shadow masking approach with Landsat and MODIS quality bands was used in order to remove pixels that could be affected by weather conditions. This is a necessary process to ensure reliability of satellite products [31,32].

## 2.3. Estimation of Land Surface Temperature (LST)

LST was estimated using Planck’s formula (Equation (1)), where  $T_B$  is the brightness temperature of Landsat 8 TIRS band 10;  $\lambda$  is the wavelength of radiance values,  $\rho$  is a constant value of 14,380 for this sensor and  $\varepsilon$  is the surface emissivity of each pixel. Lastly, LST values obtained in the Kelvin scale were converted to Celsius, subtracting 273.15. The process was conducted in the QGIS 3.16.15 raster calculator [33,34].

$$TS = \left( \frac{T_B}{1 + \left( \lambda \times \frac{T_B}{\rho} \right) \ln \varepsilon} - 273.15 \right) \quad (1)$$

Surface emissivity ( $\varepsilon$ ) was calculated with the equation developed by Sobrino et al. [35] (Equation (2)), which uses the predefined constants for the sensor of 0.986 and 0.0004, as well as the NDVI per pixel,  $NDVI_{min}$  and  $NDVI_{max}$  (maximum and minimum NDVI present within the study area).

$$\varepsilon = 0.986 + 0.0004 \times \left( \frac{NDVI - NDVI_{min}}{NDVI_{max} - NDVI_{min}} \right)^2 \quad (2)$$

## 2.4. Spectral Indices

The Soil-Adjusted Vegetation Index (*SAVI*) is used to identify areas where vegetation cover is low. The *SAVI* is calculated as a ratio between the red band (*R*), near-infrared band (*NIR*) values with a soil brightness correction factor (*L*). For the Landsat 8, this factor is a constant value of 0.5 (Equation (3)).

$$SAVI = \left( \frac{NIR - R}{NIR + R + L} \right) * (1 + L) \quad (3)$$

The Normalized Difference Vegetation Index (*NDVI*) developed by Rouse et al. [36] is a measure of photosynthetic activity and vegetation vigor. It was estimated using the red band (*R*) and near-infrared band (*NIR*) of the Landsat 8 OLI sensor (Equation (4)).

$$NDVI = \frac{R - NIR}{R + NIR} \quad (4)$$

The Vegetation Temperature Condition Index (*VTCI*) was subsequently estimated. This index has been used to monitor the spatial distribution of drought conditions. It was developed by Wang et al. [24]. *VTCI* is calculated based on Equations (5)–(7), where *LST<sub>max</sub>* and *LST<sub>min</sub>* are the maximum and minimum *LST* values for pixels with the same *NDVI* value; *a*, *b*, *a'* and *b'* are the coefficients of a linear regression between the maximum and minimum *NDVI* values with respect to *LST*.

$$VTCI = \frac{LST_{max}(NDVI_i) - LST(NDVI_i)}{LST_{max}(NDVI_i) - LST_{min}(NDVI_i)} \quad (5)$$

$$LST_{max}(NDVI_i) = a + b(NDVI_i) \quad (6)$$

$$LST_{min}(NDVI_i) = a' + b'(NDVI_i) \quad (7)$$

## 2.5. Topographic Variables

Topographic variables were derived from the Digital Elevation Model (DEM) with a 30 m spatial resolution by the Shuttle Radar Topography Mission (SRTM), which was downloaded from the US Geological Service website (<https://earthexplorer.usgs.gov>, accessed on 28 April 2022). Those variables were calculated from the DEM using the QGIS 3.16.15 software [33] (Table 4).

**Table 4.** Topographic variables.

Topographic Variable	Equation	Description
Elevation	$Elv = Z(x, y)$	Vertical distance of a point on the earth's surface above sea level. Oliver et al. [37].
Aspect	$T\theta = \arctan\left(\frac{-H}{-G}\right)$	North-facing tilt angle of the area. Horn [38].
Slope	$s = \arctan\left(\sqrt{p^2 + q^2}\right)$	Inclination to the horizontal. Oliver et al. [37].
Plane curvature	$C_W = 2 \frac{DH^2 + EG^2 - FGH}{G^2 + H^2}$	Direction of the slope with the highest angle. Zevenbergen and Thorne [39].
Wind Exposition Index	$H_L = \frac{\sum_{i=1}^n \frac{1}{ln(dLHi)} \cdot \tan^{-1}\left(\frac{dLZi}{dWHi}\right)}{\sum_{i=1}^n \frac{1}{n(dLHi)}}$	Calculates the wind effect in all directions. Böhner [40]

Where: *Z*, elevation; *p* and *q* are the components of the gradient vector of slope; *D*, *F*, *G* and *H* were derived according to the equation of Zevenbergen and Thorne [39]; *dWHi* and *dLHi* horizontal distance in windward and leeward, *dLZi* vertical distance to raster cell [40].

## 2.6. Texture Metrics

Texture variables of the *LST* layer (Table 5) were calculated from a gray level co-occurrence matrix (GLCM). This method results in different variables based on the same raster layer. Each of these variables allows contrasting specific texture properties to high-

light the image's heterogeneity [41]. Texture variables were generated for a  $3 \times 3$  kernel, using Rstudio's "glcm" package [42].

**Table 5.** Texture variables derived from GLCM.

Texture Variables	Equation	Description
Mean	$ME = \sum_{i,j=1}^{Ng} i * P(i,j)$	Mean of the probability values from GLCM. It is directly related to the spectral heterogeneity.
Variance	$SD \sqrt{\sum_{i,j=1}^{Ng} (i - u)^2 P(i,j)}$	Measure of the global variation in the image. The increase in the values, meaning higher levels of spectral heterogeneity.
Homogeneity	$HO = \sum_{i,j=0}^{N-1} i \frac{P_{i,j}}{1+i-j^2}$	Measure of the uniformity of grey-tones in the image.
Contrast	$CO = \sum_{i,j=0}^{N-1} i P_{i,j}(i,j)^2$	Quadratic measure of the local variation in the images.
Dissimilarity	$DI = \sum_{i,j=0}^{N-1} i P_{i,j}[i - j]$	Linear measure of the local variation in the image.
Entropy	$EN = \sum_{i,j=0}^{N-1} i P_{i,j}[-\ln_i - P_{i,j}]$	Measure of the disorder in the image. This measure is inversely related to the second moment.
Second moment	$SM = \sum_{i,j=0}^{N-1} i \frac{P_{i,j}^2}{I_j}$	Measure of the order in the image. It is related to the energy required for arranging the elements in the system.
Correlation	$CC = \frac{\sum_{i,j} ijP(i,j) - \mu_x \mu_y}{\sigma_x \sigma_y}$	Measure of the linear dependency between neighboring pixels.

Where:  $P(i,j)$  = Entries in a normalized gray-tone spatial-dependence matrix;  $Ng$  = Number of distinct gray levels in the quantized image.

## 2.7. Statistical Analysis

Alignment of the raster layers was conducted to standardize the spatial resolution and pixel size. This process was the starting point for the statistical analysis. With the zonal statistics plugin of the QGIS 3.16.15 software [33], the SPIFYS data were extracted with a 50-m buffer to obtain information linked to each of the predictor variables (Table 6).

**Table 6.** Predictor variables.

Variable	Equation	Resolution (m)	Units
NDVI	(4)	$30 \times 30$	-1 to 1
VTCI	(5)	$30 \times 30$	0 to 1
SAVI	(3)	$30 \times 30$	-1 to 1
LST	(1)	$30 \times 30$	°C
Evapotranspiration	[35]	$500 \times 500$	$\text{kg m}^{-2}$
Longitude		$30 \times 30$	DD
Latitude		$30 \times 30$	DD
Mean	Table 5	$30 \times 30$	-
Variance	Table 5	$30 \times 30$	-
Homogeneity	Table 5	$30 \times 30$	-
Contrast	Table 5	$30 \times 30$	-
Dissimilarity	Table 5	$30 \times 30$	-
Entropy	Table 5	$30 \times 30$	-
Second moment	Table 5	$30 \times 30$	-
Correlation	Table 5	$30 \times 30$	-
Elevation		$30 \times 30$	meters
Aspect	Table 4	$30 \times 30$	grades
Slope	Table 4	$30 \times 30$	grades
Plane curvature	Table 4	$30 \times 30$	$1/100$ of z
WEI	Table 4	$30 \times 30$	5 to -5

Where: NDVI = Normalized Difference Vegetation Index; VTCI = Vegetation Temperature Condition Index; LST = Land Surface Temperature; WEI = Wind Exposition Index.

A Pearson's correlation analysis ( $r$ ) was used to identify variables most linked to AGB. Lastly, a multicollinearity analysis between variables was conducted using the variance inflation factor (VIF). Variables with a VIF value above 10 were removed, as this means that there is collinearity with some other variable [1,43].

Once variables were selected, a GAM was performed, i.e., a semi-parametric model that allows linear and non-linear responses of the predictor variables based on a dependent variable to be analyzed. GAM models have been successfully used to analyze AGB values and forest structure with data from remote sensing [25,26]. GAM regression was conducted in RStudio with the "mgcv" package [44,45].

The deviance explained values and the Akaike information criterion (AIC) were obtained, which analyzes the relevance and fit of a model based on complexity; a lower AIC value means a better fit in the model [46]. In addition, a prediction map was made using the *layerstack* of the previously selected predictor variables as input.

The coefficient of determination ( $R^2$ ) and the root-mean-square error (RMSE) were estimated using Equations (8) and (9), where  $y_i$  is the AGB value observed in the field,  $\hat{y}_i$  is the value estimated by the model,  $\bar{y}_i$  the average AGB,  $n$  the number of observations and  $p$  the number of model parameters.  $R^2$  and RMSE data allowed the goodness of fit of evaluation models to be quantified:

$$R^2 = 1 - \frac{\sum_{i=1}^n (y_i - \hat{y}_i)^2}{\sum_{i=1}^n (\bar{y}_i - \hat{y}_i)^2} \quad (8)$$

$$RMSE = \sqrt{\frac{\sum_{i=1}^n (y_i - \hat{y}_i)^2}{n - p}} \quad (9)$$

Likewise, a verification of the model was carried out, using an independent field dataset ( $n = 50$ ), in order to evaluate the AGB predicted from the model values.

### 3. Results

Pearson's correlation analysis showed that AGB had a negative relationship with LST, which was stronger in spring ( $r = -0.58$ ). As for NDVI and VTCI, a positive relationship was observed, which was also stronger in spring ( $r = 0.63$  and  $r = 0.32$ ) (Figure 2). ET showed a weak positive relationship, although it becomes slightly stronger in winter ( $r = 0.43$ ). Regarding the texture variables, the mean and variance variables showed the highest positive correlation. Lastly, the topographic variables with the highest AGB correlation (Figure 3) were altitude ( $r = -0.12$ ), slope ( $r = 0.10$ ) and curvature ( $r = 0.10$ ). The GAM model was built with the highest AGB correlation (positive or negative) variables.

Most predictor variables and AGB showed a non-linear relationship. The variables GLCM\_mean, longitude, latitude, LST, VTCI, NDVI, ET, were significant ( $p < 0.001$ ), and explained between 10.6% and 48.1% of the total variance (Table 7). In addition, four interactions between two variables were tested. All tested interactions were significant ( $p < 0.001$ ), with percentages of deviance explained ranging from 33% to 36.6% (Table 8). Three out of these interactions were considered as potential GAM components.

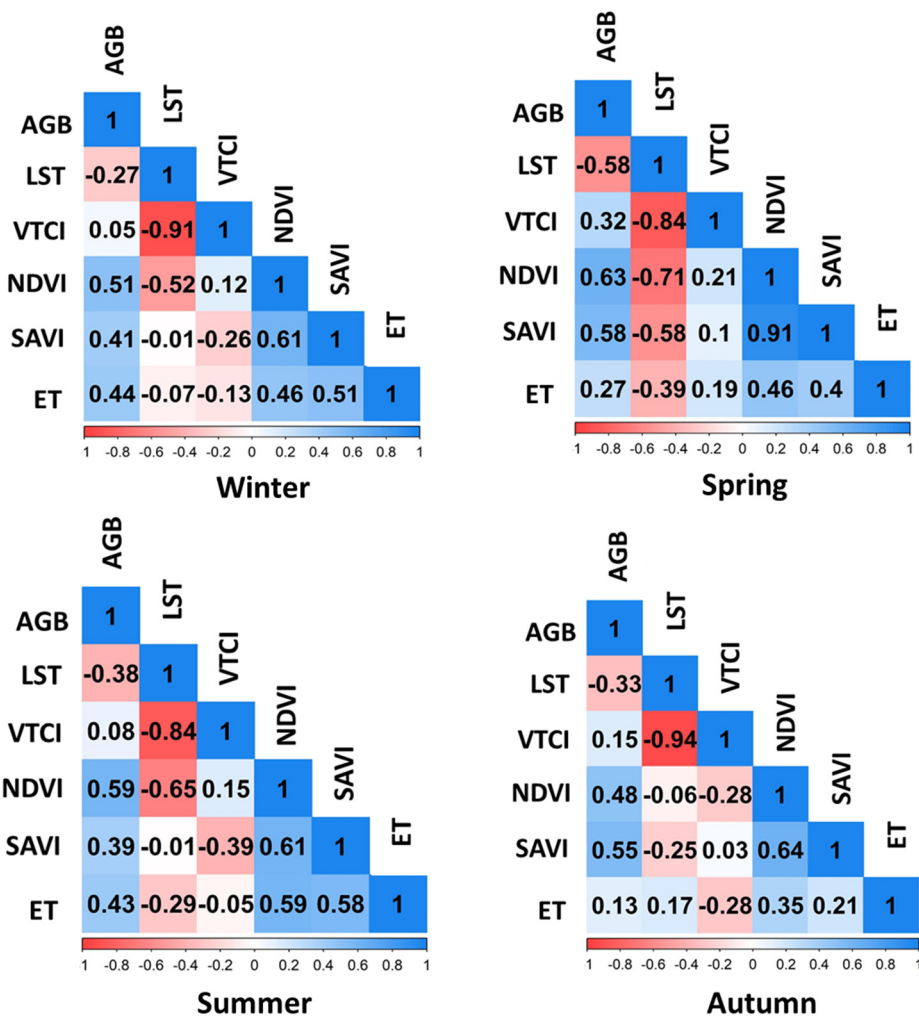


**Figure 2.** Pearson's correlation between predictor spectral variables and above-ground biomass (AGB) in different seasons of the year. LST, Land Surface Temperature ( $^{\circ}\text{C}$ ); VTCI, Vegetation Temperature Condition Index; NDVI, Normalized Difference Vegetation Index; SAVI, Soil-adjusted vegetation index; ET, evapotranspiration ( $\text{kg m}^{-2}$ ).

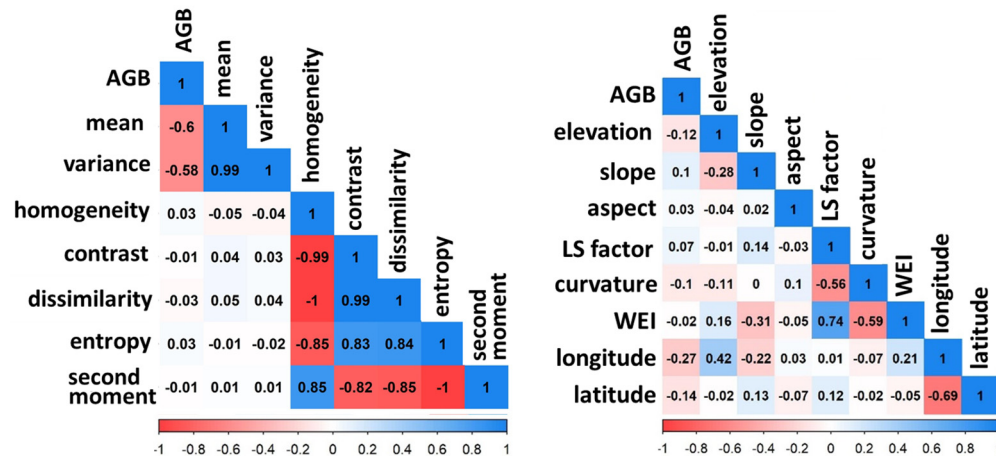


**Figure 3.** Pearson's correlation between predictor texture of Grey-Level Co-Occurrence Matrix, topographic and spatial variables and above-ground biomass (AGB); these variables do not change throughout the year. WEI, Wind Exposition Index; AGB ( $\text{Mg ha}^{-1}$ ), elevation (m), slope ( $^{\circ}$ ), longitude (DD), latitude (DD).

**Table 7.** Individual effects of variables on AGB in GAM models.

Variable	edf	Residual_df	Deviance Explained	Adjusted R <sup>2</sup>	p-Value
NDVI	3.08	3.99	48.1%	0.469	<0.001
LST	6.32	8.04	38.9%	0.384	<0.001
GLCM_mean	2.73	3.46	34.9%	0.342	<0.001
SAVI	1.38	1.67	34.0%	0.336	<0.001
GLCM_variance	1.86	2.36	34.0%	0.335	<0.001
Lon	6.50	7.62	24.3%	0.223	<0.001
Lat	8.13	8.77	21.8%	0.192	<0.001
ET	1.00	1.00	12.5%	0.113	<0.001
VTCI	9.29	11.05	10.6%	0.101	<0.001
Curvature	1.95	2.52	3.30%	0.021	0.125
Elevation	1.93	2.45	2.78%	0.020	0.057

Where: edf = effective degrees of freedom; Lon = longitude (DD); Lat = latitude (DD); LST = Land Surface Temperature ( $^{\circ}$ C); ET = evapotranspiration ( $\text{kg} \cdot \text{m}^{-2}$ ); Slope ( $^{\circ}$ ); Elevation (m); GLCM = Grey-Level Co-Occurrence Matrix.

**Table 8.** Interactions of significant variables on AGB in GAMs.

Interaction Terms	edf	Residual_df	Deviance Explained	R <sup>2</sup>	p-Value
LST-Elevation	2.87	3.52	36.6%	0.39	<0.001
LST-ET	9.85	13.21	36%	0.35	<0.001
Lon-Lat	11.94	15.58	33%	0.30	<0.001
LST-Slope	4.27	5.83	30.5%	0.27	<0.001

Where: edf = effective degrees of freedom; Lon = longitude (DD); Lat = latitude (DD); LST = Land Surface Temperature ( $^{\circ}$ C); ET = evapotranspiration ( $\text{kg} \cdot \text{m}^{-2}$ ); Slope ( $^{\circ}$ ); Elevation (m).

### Model Optimization

Variables and interactions were added to the model, and the deviance explained; RMSE and AIC value were evaluated to determine whether adding a variable improved a model's performance. From the six models tested, model six showed a higher explanatory rate (61.0%) with lower RMSE and AIC (28.33 Mgha $^{-1}$  and 1994.34) (Table 9).

**Table 9.** Analysis of deviation in a forward selection regression process in six above-ground biomass (AGB) models.

No	Model Structure	Deviance Explained	AIC	RMSE
1	AGB = s(lon,lat) + s(LST) + s(VTCI) + s(ET) + s(Elevation) + s(slope) + s(GLCM_mean)	53.7%	2005.72	30.88
2	AGB = s(lon,lat) + s(NDVI) + s(Elevation) + s(slope) + s(GLCM_mean)	56.8%	2005.72	30.01
3	AGB = s(lon,lat) + s(VTCI) + s(NDVI) + s(ET) + s(Elevation) + s(slope) + s(GLCM_mean)	56.8%	1998.27	29.81
4	AGB = s(lon,lat) + s(NDVI) + s(ET) + s(Elevation) + s(slope) + s(GLCM_mean)	56.3%	1995.56	29.80
5	AGB = s(lon,lat) + s(LST) + s(VTCI) + s(NDVI) + s(ET) + s(Elevation) + s(slope) + s(GLCM_mean)	60.2%	1996.01	29.41
6	AGB = s(lon,lat) + s(LST,ET) + s(LST, Elevation) + s(VTCI) + s(NDVI) + s(slope) + s(GLCM_mean)	61.0%	1994.34	28.33

Where: Lon = longitude (DD); Lat = latitude (DD); LST = Land Surface Temperature ( $^{\circ}$ C); VTCI = Vegetation Temperature Condition Index; NDVI = Normalized Difference Vegetation Index; ET = evapotranspiration ( $\text{kg} \cdot \text{m}^{-2}$ ); GLCM = Grey-Level Co-Occurrence Matrix; Slope ( $^{\circ}$ ); Elevation (m).

The graphs of each variable against AGB show that VTCI has an increasing linear relationship. On the other hand, GLCM\_mean had a decreasing linear relationship, while NDVI and Slope showed an initially increasing relationship and tended to decrease as

AGB increased (Figure 4a–d). The “Longitude, Latitude” interaction showed that areas with increased AGB are linked to western and southern Durango’s forests. Meanwhile, the amount of AGB increases in areas with lower LST and ET. Finally, the “LST, DEM” interaction showed a positive relationship with AGB in areas with lower temperature and lower elevation (Figure 5).

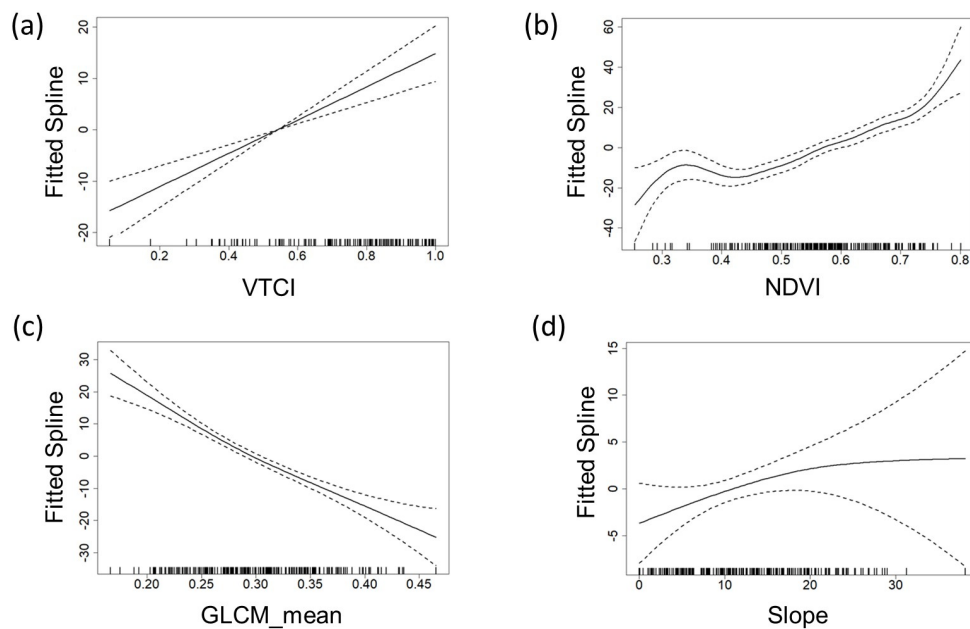


**Figure 4.** Explanatory variables with significant contribution to the respective binomial response variables. Each plot shows the relationship of the fitted function to the response and scaled to zero. The plots include approximate 95% pointwise. VTCI, Vegetation Temperature Condition Index; NDVI, Normalized Difference Vegetation Index; GLCM\_mean, mean of Grey-Level Co-Occurrence Matrix.

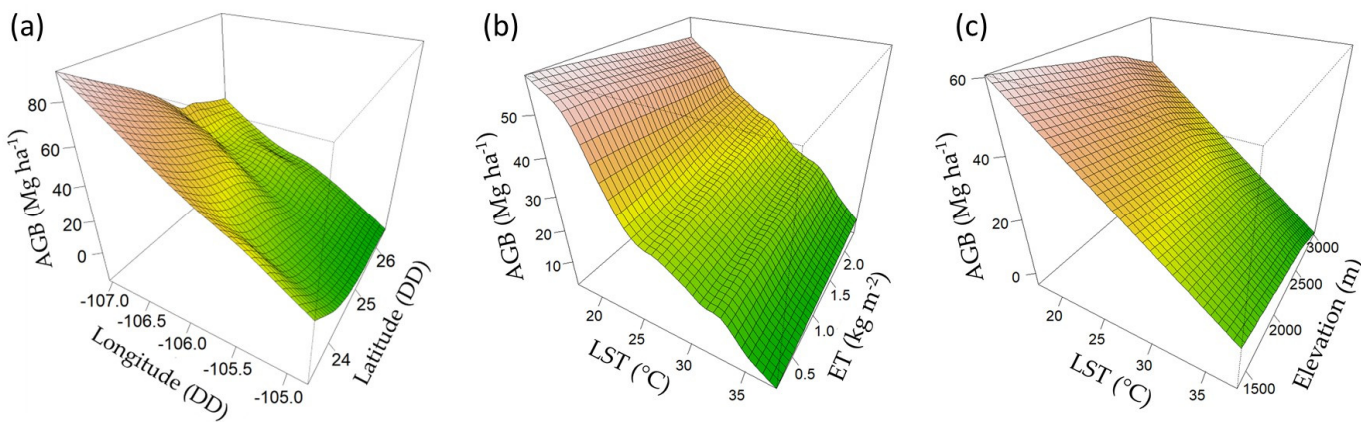


**Figure 5.** Responses of AGB to the interaction of two variables. (a) Latitude and Longitude, (b) Land surface temperature (LST) and evapotranspiration (ET) and (c) Land surface temperature (LST) and Elevation.

Model diagnostic plots (Figure 6) generally help to understand the model performance. The QQ plot (Figure 6a) shows a normal distribution slightly skewed to the right with long tails, while the residual plot (Figure 6b) confirms independence of the residuals with a slight increase in error variability as the AGB amount increases. The residual distribution plot shows a marked tendency to a normal distribution (Figure 6c), and the overlay plot of the model’s response data and fitted values indicate a moderate model efficiency (Figure 6d). Lastly, an AGB prediction map was generated by applying the selected model (Figure 7).

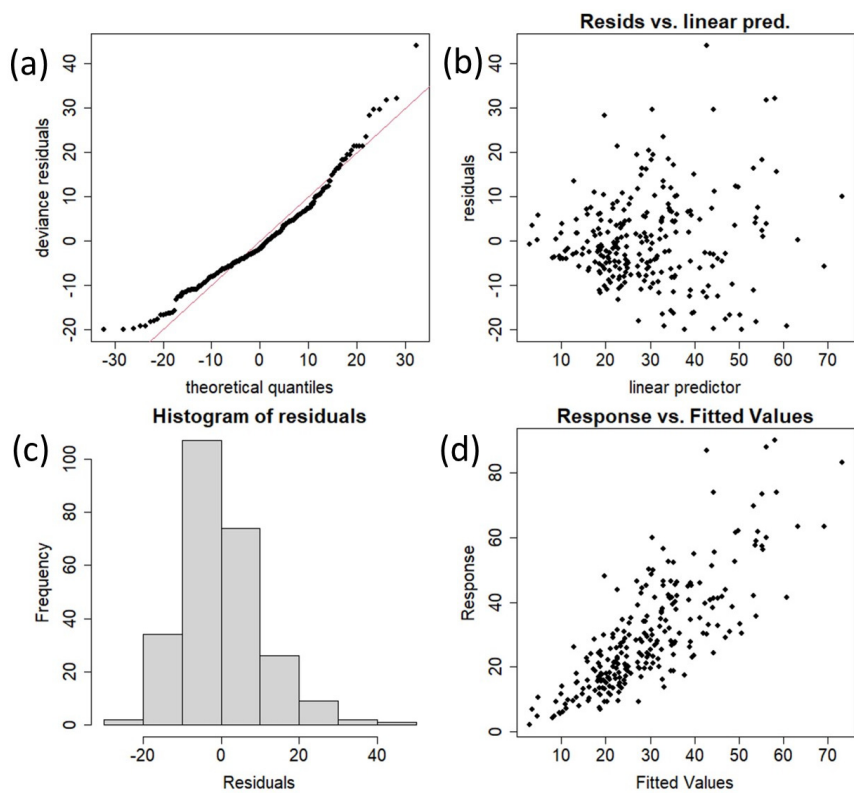


**Figure 6.** Diagnostic plots of generalized additive model (model six, see Table 9). (a) Q-Q plot, (b) residual plot, (c) density plot of residuals, (d) fitted values plotted against response variables.

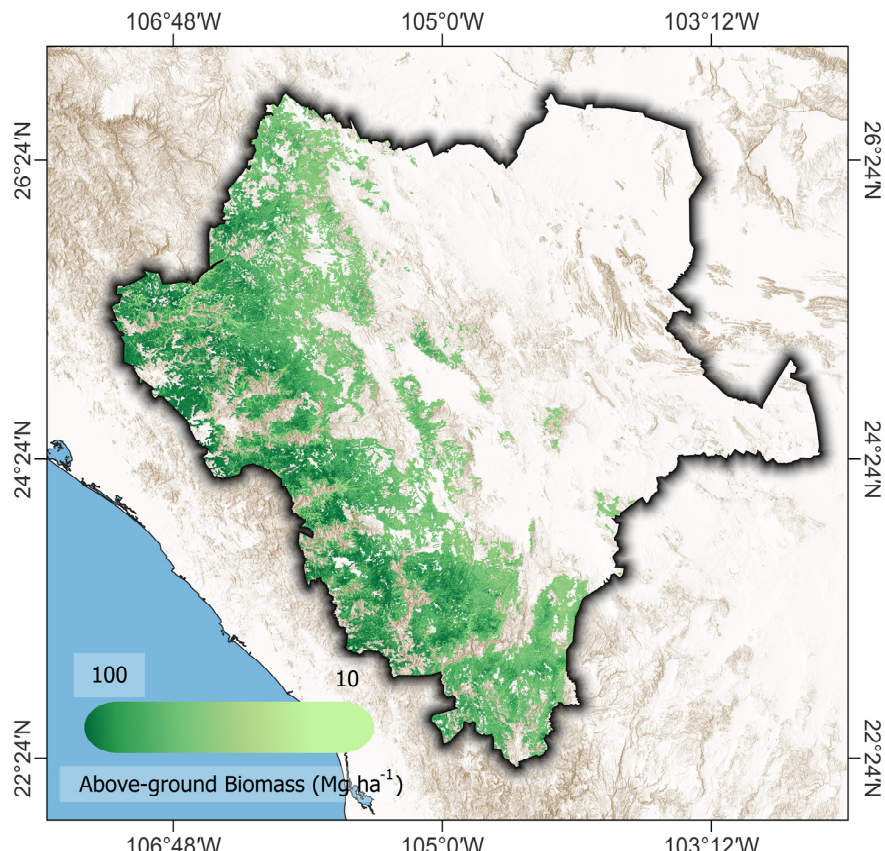


**Figure 7.** Predicted above-ground biomass ( $\text{Mg ha}^{-1}$ ) in the temperate forest of Durango, Mexico, generated from model six (Table 9).

Finally, Table 10 shows the descriptive statistics and adjustment statistics of the verification of the GAM model through the application of the model to 50 AGB data derived from SPIFyS independent of the dataset used to generate the GAM model.

**Table 10.** Independent verification of the general model to estimate AGB ( $\text{Mg ha}^{-1}$ ).

Estimated AGB	Num. of Observations	Min	Max	Mean	SD	R <sup>2</sup>	RMSE
GAM calibration	318	2.05	92.33	30.82	18.00	0.61	28.33
Independent verification	50	4.79	83.25	27.23	18.15	0.58	31.21

Where: Min = minimum value; Max = maximum value; Mean = mean value; SD = Standard deviation.

#### 4. Discussion

Interactions between biological and environmental aspects often have complex behaviors (i.e., different from linear), so a model's predictive capacity depends largely on the flexibility to identify non-linear relationships [47]. GAM models are capable of identifying linear and non-linear relationships. Smoothing terms allow for the adjusting of unusual variance patterns that a linear model would not detect, making it possible to visualize and add the contribution of each variable to the plugins [48]. For this paper, GAM modeling was useful to estimate the AGB amount in the temperate forests of Durango, Mexico.

A correlation analysis allowed selecting predictive variables that were subsequently entered into the GAM model. One of the main challenges faced by spatial models is parsimony, [49,50] i.e., models with the least number of predictors, which in turn achieve reasonable estimates. In this paper, a model with moderate precision was developed; however, the number of variables (nine) allows the estimation process to be simpler.

Our observed negative relationship with LST seems to support previous observations that LST tends to increase in degraded forest ecosystems or ecosystems with forest loss [51]. For example, Özkan et al. [52], in a study conducted in forests in Turkey, found that areas with tree cover showed a decrease of  $1.14^{\circ}\text{C}$  compared to surfaces with herbaceous vegetation. Because forest structure parameters, such as canopy density, are closely related to the AGB amount [53], so an LST–AGB relationship could be expected.

Teofano et al. [54] analyzed the relation of AGB with indexes vegetation of a forest plantation; they figured out that this relation changes through the year and it is related with the phenostage, the growth stage that shows the weakest relation. Likewise, our results showed that the AGB–LST relationship had variations from the phenological changes of the plant community throughout the year. The AGB–LST relationship becomes stronger in spring, which could be explained by higher temperatures and less precipitation this season, resulting in a more marked contrast between the temperature of the bare soil or with herbaceous vegetation and areas with high forest density [51].

NDVI is the most widely used spectral index for vegetation analysis. It is a plant vigor proxy that measures photosynthetic activity [55]. Our results support the AGB–NDVI relationship described in different studies [9,13,56]. Although the variable with the highest deviance explained percentage was NDVI, the addition of variables such as LST and VTCI improved the model efficiency, so they could be considered as potential variables to be included in AGB models [17].

While VTCI describes regional drought conditions, this index was created considering LST changes that occur in vegetation, due to stomatal closure caused by drought stress [24,57]. Forest ecosystems with lower density or under fragmentation processes are more susceptible to drought stress [58]. The water stress is highly correlated with AGB due to less water availability and is related with populations with lower rates of AGB increase [59]. Furthermore, drought stress events have a negative impact on biomass, as they usually cause massive tree mortality, and favor conditions that can result in forest fires [60].

Several studies have used GLCM features as variables of parametric and non-parametric models [10,61–63]. Iqbal et al. [62] assess GLCM variables to classify different types of crops; they concluded that GLCM features improved by 13.65% the accuracy of the analysis. In the present study, of the GLCM texture variables of the temperature layer, only GLCM-mean was selected, as this variable managed to highlight the heterogeneity in the raster layer and in turn improved the predictive capacity of the dependent variable (AGB).

The Longitude–Latitude interaction was deemed as an influential variable for the productivity of an ecosystem. These spatial variables greatly favor the site's climatic characteristics (e.g., solar incidence, wind currents, humidity) that determine the photosynthetic and plant respiration processes [21,64–66]. Our observed lower biomass in northern latitudes agrees with the findings of Gillman et al. [65], who observed that a negative relationship of latitude with Net Primary Productivity on a global scale. In addition, a higher biomass concentration is observed in the extreme west of Durango state, near the Pacific Ocean, a transition zone with tropical deciduous forest [67,68].

The ET–LST interaction showed that, in areas with lower evapotranspiration and temperature, a greater AGB amount is found. Forest cover largely regulates local temperature through the release of water vapor (transpiration), energy and energy exchange between the canopy surface and the atmosphere [69]. ET is deemed as one of the most important LST-shaping mechanisms [70]. Although higher ET rates would be expected in more productive ecosystems, some papers mention that this relationship changes throughout the year; for example, Strilesky et al. [71] analyzed the relationship between biomass and ET in a forest ecosystem, finding that a greater biomass amount does not lead to higher ET levels throughout the year, since forest ecosystems with higher biomass show lower ET in dry months. Our observed stronger relationship with spring water stress indicators seem to support those seasonal variations in the relationships between ET and AGB.

The elevation and LST relationship allowed identifying a greater amount of AGB in areas with medium elevation (1500–2000 m). The middle zone of mountainous ecosystems has a greater amount of precipitation and therefore a higher environmental humidity [72], which results in a temperature decrease. For example, Liu et al. [72] observed that the middle zone of a mountainous ecosystem in China had a forest structure with a denser canopy and a higher carbon sequestration capacity. In addition, the increase in elevation has a negative relationship with the amount of biomass, as the increase in altitude is related to the decrease in soil water content [64,73]. The decrease in biomass at the upper altitude threshold is explained by the species-energy theory, which indicates that, in more extreme conditions, species tend to reduce their growing seasons length and have slower metabolic processes, as observed in stands with lower AGB [66,74]. This research focused on temperate forest; however, in future research it would be interesting to analyze these relationships for other types of vegetation with a model such as the one developed in this document. This would allow more potential uses of LST and ET to be identified in the monitoring of forest resources.

## 5. Conclusions

The results of the current study showed that the use of GAM models could be adequate for AGB estimation from remote sensed temperature, water stress and other variables in temperate forests of Durango, Mexico. Variables such as LST, ET and VTCI combined with topographic and texture parameters were shown to be useful to understand change processes in terms of AGB productivity and quantity in temperate forests. AGB and LST showed a negative and variable correlation throughout the year. This relationship was clearer in spring ( $r = -0.58$ ). This seems to indicate that the LST data has greater predictive potential for AGB in seasons when there is less precipitation and higher temperature, resulting in a greater contrast between higher and lower AGB plots.

In future studies, it would be useful to analyze the potential of satellite data available from previous decades to understand AGB dynamics across space and time in temperate forests such as the ones at the state of Durango, Mexico.

**Author Contributions:** P.M.L.-S. and M.R.-C. planned and designed the research; M.R.-C. and P.M.L.-S. contributed to data analysis; and P.M.L.-S. led the manuscript with contributions from M.R.-C. and D.J.V.-N.; M.R.-C. writing—original draft preparation, dasometric database resources J.J.C.-R., J.C.H.-D., C.W. and D.J.V.-N. writing—review and editing. All authors have read and agreed to the published version of the manuscript.

**Funding:** This research received no external funding.

**Data Availability Statement:** The data presented in this study are available on request from the corresponding author.

**Acknowledgments:** The authors are grateful to the Mexican National Science and Technology Council (CONACYT) for supporting the studies of the first author. We are also grateful for the careful review and valuable comments by the anonymous reviewers.

**Conflicts of Interest:** The authors declare no conflict of interest.

## References

1. Jiang, F.; Kutia, M.; Ma, K.; Chen, S.; Long, J.; Sun, H. Estimating the Aboveground Biomass of Coniferous Forest in Northeast China Using Spectral Variables, Land Surface Temperature and Soil Moisture. *Sci. Total Environ.* **2021**, *785*, 147335. [[CrossRef](#)] [[PubMed](#)]
2. Temesgen, H.; Affleck, D.; Poudel, K.; Gray, A.; Sessions, J. A Review of the Challenges and Opportunities in Estimating above Ground Forest Biomass Using Tree-Level Models. *Scand. J. For. Res.* **2015**, *30*, 326–335. [[CrossRef](#)]
3. Watson, R.T.; Noble, I.R.; Bolin, B.; Ravindranath, N.H.; Verardo, D.J.; Dokken, D.J. *Land Use, Land-Use Change and Forestry*; Cambridge University Press: Cambridge, UK, 2000.
4. Pantaleo, Y. Tropical Reinforest above Ground Biomass and Carbon Stock Estimation for Upper and Lower Canopies Using Terrestrial Laser Scanner and Canopy Height Model from Unmanned Aerial Vehicle (UAV) Imagery in Ayer-Hitam, Malaysia. Master’s Thesis, University of Twente, Enschede, The Netherlands, 2017; 5p.
5. Kumar, L.; Mutanga, O. Remote Sensing of Above-Ground Biomass. *Remote Sens.* **2017**, *9*, 935. [[CrossRef](#)]
6. Holl, K.D.; Zahawi, R.A. Factors Explaining Variability in Woody Above-Ground Biomass Accumulation in Restored Tropical Forest. *For. Ecol. Manag.* **2014**, *319*, 36–43. [[CrossRef](#)]
7. Ravindranath, N.H.; Ostwald, M. Carbon Pools and Measurement Frequency for Carbon Inventory. In *Carbon Inventory Methods Handbook for Greenhouse Gas Inventory, Carbon Mitigation and Roundwood Production Projects*; Springer: Dordrecht, The Netherlands, 2008; pp. 31–44. ISBN 978-1-4020-6547-7.
8. Rodríguez-Veiga, P.; Wheeler, J.; Louis, V.; Tansey, K.; Balzter, H. Quantifying Forest Biomass Carbon Stocks From Space. *Curr. For. Rep.* **2017**, *3*, 1–18. [[CrossRef](#)]
9. Zhu, X.; Liu, D. Improving Forest Aboveground Biomass Estimation Using Seasonal Landsat NDVI Time-Series. *ISPRS J. Photogramm. Remote Sens.* **2015**, *102*, 222–231. [[CrossRef](#)]
10. López-Serrano, P.M.; Cárdenas Domínguez, J.L.; Corral-Rivas, J.J.; Jiménez, E.; López-Sánchez, C.A.; Vega-Nieva, D.J. Modeling of Aboveground Biomass with Landsat 8 OLI and Machine Learning in Temperate Forests. *Forests* **2020**, *11*, 11. [[CrossRef](#)]
11. Zeng, Y.; Hao, D.; Huete, A.; Dechant, B.; Berry, J.; Chen, J.M.; Joiner, J.; Frankenberg, C.; Bond-Lamberty, B.; Ryu, Y.; et al. Optical Vegetation Indices for Monitoring Terrestrial Ecosystems Globally. *Nat. Rev. Earth Environ.* **2022**, *3*, 477–493. [[CrossRef](#)]
12. Meneses-Tovar, C.L. NDVI as Indicator of Degradation. *Unasylva* **2011**, *62*, 39–46.
13. Vaglio Laurin, G.; Pirotti, F.; Callegari, M.; Chen, Q.; Cuozzo, G.; Lingua, E.; Notarnicola, C.; Papale, D. Potential of ALOS2 and NDVI to Estimate Forest Above-Ground Biomass, and Comparison with Lidar-Derived Estimates. *Remote Sens.* **2016**, *9*, 18. [[CrossRef](#)]
14. Günlü, A.; Ercanlı, I.; Başkent, E.Z.; Çaklı, G. Estimating Aboveground Biomass Using Landsat TM Imagery: A Case Study of Anatolian Crimean Pine Forests in Turkey. *Ann. For. Res.* **2014**, *57*, 289–298.
15. Kelsey, K.; Neff, J. Estimates of Aboveground Biomass from Texture Analysis of Landsat Imagery. *Remote Sens.* **2014**, *6*, 6407–6422. [[CrossRef](#)]
16. García-Santos, V.; Cuxart, J.; Martínez-Villagrasa, D.; Jiménez, M.A.; Simó, G. Comparison of Three Methods for Estimating Land Surface Temperature from Landsat 8-TIRS Sensor Data. *Remote Sens.* **2018**, *10*, 1450. [[CrossRef](#)]
17. Van Leeuwen, T.T.; Frank, A.J.; Jin, Y.; Smyth, P.; Goulden, M.L.; van der Werf, G.R.; Randerson, J.T. Optimal Use of Land Surface Temperature Data to Detect Changes in Tropical Forest Cover. *J. Geophys. Res. Biogeosci.* **2011**, *116*, G02002. [[CrossRef](#)]
18. Pongratz, J.; Bounoua, L.; DeFries, R.S.; Morton, D.C.; Anderson, L.O.; Mauser, W.; Klink, C.A. The Impact of Land Cover Change on Surface Energy and Water Balance in Mato Grosso, Brazil. *Earth Interact.* **2006**, *10*, 1–17. [[CrossRef](#)]
19. Rosas-Chavoya, M.; López-Serrano, P.M.; Vega-Nieva, D.J.; Wehenkel, C.A.; Hernández-Díaz, J.C. Application of Land Surface Temperature from Landsat Series to Monitor and Analyze Forest Ecosystems: A Bibliometric Analysis. *For. Syst.* **2022**, *31*, e021. [[CrossRef](#)]

20. Jaramillo, F.; Cory, N.; Arheimer, B.; Laudon, H.; van der Velde, Y.; Hasper, T.B.; Teutschbein, C.; Uddling, J. Dominant Effect of Increasing Forest Biomass on Evapotranspiration: Interpretations of Movement in Budyko Space. *Hydrol. Earth Syst. Sci.* **2018**, *22*, 567–580. [[CrossRef](#)]
21. Ali, A.; Lin, S.-L.; He, J.-K.; Kong, F.-M.; Yu, J.-H.; Jiang, H.-S. Elucidating Space, Climate, Edaphic, and Biodiversity Effects on Aboveground Biomass in Tropical Forests. *Land Degrad. Dev.* **2019**, *30*, 918–927. [[CrossRef](#)]
22. Mu, Q.; Heinsch, F.A.; Zhao, M.; Running, S.W. Development of a Global Evapotranspiration Algorithm Based on MODIS and Global Meteorology Data. *Remote Sens. Environ.* **2007**, *111*, 519–536. [[CrossRef](#)]
23. Nguyen, H.; Wheeler, M.C.; Otkin, J.A.; Cowan, T.; Frost, A.; Stone, R. Using the Evaporative Stress Index to Monitor Flash Drought in Australia. *Environ. Res. Lett.* **2019**, *14*, 64016. [[CrossRef](#)]
24. Wang, P.; Li, X.; Gong, J.; Song, C. Vegetation Temperature Condition Index and Its Application for Drought Monitoring. In Proceedings of the IGARSS 2001. Scanning the Present and Resolving the Future. Proceedings. IEEE 2001 International Geoscience and Remote Sensing Symposium (Cat. No.01CH37217), Sydney, Australia, 9–13 July 2001; Volume 1, pp. 141–143.
25. Soriano-Luna, M.D.L.Á.; Ángeles-Pérez, G.; Guevara, M.; Birdsey, R.; Pan, Y.; Vaquera-Huerta, H.; Valdez-Lazalde, J.R.; Johnson, K.D.; Vargas, R. Determinants of Above-Ground Biomass and Its Spatial Variability in a Temperate Forest Managed for Timber Production. *Forests* **2018**, *9*, 490. [[CrossRef](#)]
26. Mikeladze, G.; Gavashelishvili, A.; Akobia, I.; Metreveli, V. Estimation of Forest Cover Change Using Sentinel-2 Multi-Spectral Imagery in Georgia (the Caucasus). *iForest* **2020**, *13*, 329–335. [[CrossRef](#)]
27. Novo-Fernández, A.; Franks, S.; Wehenkel, C.; López-Serrano, P.M.; Molinier, M.; López-Sánchez, C.A. Landsat Time Series Analysis for Temperate Forest Cover Change Detection in the Sierra Madre Occidental, Durango, Mexico. *Int. J. Appl. Earth Obs. Geoinf.* **2018**, *73*, 230–244. [[CrossRef](#)]
28. Corral-Rivas, J.J.; Vargas-Larreta, B.; Wehenkel, C.; Aguirre-Calderón, O.A.; Crecente-Campo, F. *Guía Para El Establecimiento, Seguimiento y Evaluación de Sitios Permanentes de Monitoreo En Paisajes Productivos Forestales*; CONAFOR: Durango, Mexico, 2013; 10p.
29. Vargas-Larreta, B.; López-Sánchez, C.A.; Corral-Rivas, J.J.; López-Martínez, J.O.; Aguirre-Calderón, C.G.; Álvarez-González, J.G. Allometric Equations for Estimating Biomass and Carbon Stocks in the Temperate Forests of North-Western Mexico. *Forests* **2017**, *8*, 269. [[CrossRef](#)]
30. U.S. Geological Survey. Earth Resources Observation and Science (EROS) Center Science Processing Architecture (ESPA) on Demand Interface (Version 5.4). Available online: <https://www.usgs.gov/media/files/eros-science-processing-architecture-demand-interface-user-guide> (accessed on 16 September 2022).
31. Mu, Q.; Zhao, M.; Running, S.W. Improvements to a MODIS Global Terrestrial Evapotranspiration Algorithm. *Remote Sens. Environ.* **2011**, *115*, 1781–1800. [[CrossRef](#)]
32. Parastatidis, D.; Mitraka, Z.; Chrysoulakis, N.; Abrams, M. Online Global Land Surface Temperature Estimation from Landsat. *Remote Sens.* **2017**, *9*, 1208. [[CrossRef](#)]
33. QGIS Development Team QGIS Geographic Information System; Open Source Geospatial. 2021. Available online: <http://qgis.org> (accessed on 10 February 2022).
34. Rosas-Chavoya, M.; Gallardo-Salazar, J.L.; López-Serrano, P.M.; Alcántara-Concepción, P.C.; León-Miranda, A.K. QGIS a Constantly Growing Free and Open-Source Geospatial Software Contributing to Scientific Development. *Cuad. De Investig. Geográfica* **2022**, *48*, 197–213. [[CrossRef](#)]
35. Sobrino, J.A.; Raissouni, N.; Li, Z.-L. A Comparative Study of Land Surface Emissivity Retrieval from NOAA Data. *Remote Sens. Environ.* **2001**, *75*, 256–266. [[CrossRef](#)]
36. Rouse, J.H.; Haas, R.H.; Schell, J.A.; Deering, D.W. Monitoring Vegetation Systems in the Great Plains with ERTS. In *Third Earth Resources Technology Satellite-1 Symposium*; Freden, S.C., Mercanti, E.P., Becker, M., Eds.; NASA: Washington, DC, USA, 1974; Volume I.
37. Oliver, M.A.; Webster, R. Kriging: A Method of Interpolation for Geographical Information Systems. *Int. J. Geogr. Inf. Syst.* **1990**, *4*, 313–332. [[CrossRef](#)]
38. Horn, B.K.P. Hill Shading and the Reflectance Map. *Proc. IEEE* **1981**, *69*, 14–47. [[CrossRef](#)]
39. Zevenbergen, L.W.; Thorne, C.R. Quantitative Analysis of Land Surface Topography. *Earth Surf. Process. Landf.* **1987**, *12*, 47–56. [[CrossRef](#)]
40. Böhner, J.; Antonić, O. Chapter 8 Land-Surface Parameters Specific to Topo-Climatology. In *Geomorphometry*; Hengl, T., Reuter, H.I., Eds.; Developments in Soil Science; Elsevier: Amsterdam, The Netherlands, 2009; Volume 33, pp. 195–226.
41. Rahimi, E.; Barghjelveh, S.; Dong, P. Quantifying How Urban Landscape Heterogeneity Affects Land Surface Temperature at Multiple Scales. *J. Ecol. Env.* **2021**, *45*, 1–13. [[CrossRef](#)]
42. Zvoleff, A. Package Glcm. R Package Version 1.6.5. 2020. Available online: <https://cran.r-project.org/web/packages/glcm> (accessed on 12 October 2021).
43. Chen, W.; Zhang, S.; Li, R.; Shahabi, H. Performance Evaluation of the GIS-Based Data Mining Techniques of Best-First Decision Tree, Random Forest, and Naïve Bayes Tree for Landslide Susceptibility Modeling. *Sci. Total Environ.* **2018**, *644*, 1006–1018. [[CrossRef](#)] [[PubMed](#)]
44. R Core Team. *R: A Language and Environment for Statistical Computing*; R Core Team: Vienna, Austria, 2021.
45. Wood, N.S. *Generalized Additive Models*, 2nd ed.; Chapman and Hall/CRC: New York, NY, USA, 2017.

46. Terrer, C.; Phillips, R.P.; Hungate, B.A.; Rosende, J.; Pett-Ridge, J.; Craig, M.E.; van Groenigen, K.J.; Keenan, T.F.; Sulman, B.N.; Stocker, B.D.; et al. A Trade-off between Plant and Soil Carbon Storage under Elevated CO<sub>2</sub>. *Nature* **2021**, *591*, 599–603. [CrossRef] [PubMed]
47. Levine, J.; de Valpine, P.; Battles, J. Generalized Additive Models Reveal Among-Stand Variation in Live Tree Biomass Equations. *Can. J. For. Res.* **2021**, *51*, 546–564. [CrossRef]
48. Frescino, T.S.; Edwards, T.C.; Moisen, G.G. Modeling Spatially Explicit Forest Structural Attributes Using Generalized Additive Models. *J. Veg. Sci.* **2001**, *12*, 15. [CrossRef]
49. Latifi, H.; Fassnacht, F.; Koch, B. Forest Structure Modeling with Combined Airborne Hyperspectral and LiDAR Data. *Remote Sens. Environ.* **2012**, *121*, 10–25. [CrossRef]
50. Toledo, R.M.; Santos, R.F.; Baeten, L.; Perring, M.P.; Verheyen, K. Soil Properties and Neighbouring Forest Cover Affect Above-Ground Biomass and Functional Composition during Tropical Forest Restoration. *Appl. Veg. Sci.* **2018**, *21*, 179–189. [CrossRef]
51. Hasnat, G.N.T. A Time Series Analysis of Forest Cover and Land Surface Temperature Change Over Dudukuria-Dhopachari Wildlife Sanctuary Using Landsat Imagery. *Front. For. Glob. Chang.* **2021**, *4*, 687988. [CrossRef]
52. Özkan, U.; Gökbulak, F. Effect of Vegetation Change from Forest to Herbaceous Vegetation Cover on Soil Moisture and Temperature Regimes and Soil Water Chemistry. *CATENA* **2017**, *149*, 158–166. [CrossRef]
53. Alrutz, M.; Gómez Díaz, J.A.; Schneidewind, U.; Krömer, T.; Kreft, H. Forest Structural Parameters and Aboveground Biomass in Old-Growth and Secondary Forests along an Elevational Gradient in Mexico. *Bot. Sci.* **2021**, *100*, 67–85. [CrossRef]
54. Theofanous, N.; Chrysafis, I.; Mallinis, G.; Domakinis, C.; Verde, N.; Siahalou, S. Aboveground Biomass Estimation in Short Rotation Forest Plantations in Northern Greece Using ESA’s Sentinel Medium-High Resolution Multispectral and Radar Imaging Missions. *Forests* **2021**, *12*, 902. [CrossRef]
55. Huang, S.; Tang, L.; Hupy, J.P.; Wang, Y.; Shao, G. A Commentary Review on the Use of Normalized Difference Vegetation Index (NDVI) in the Era of Popular Remote Sensing. *J. For. Res.* **2021**, *32*, 1–6. [CrossRef]
56. Wang, Y.; Shen, X.; Jiang, M.; Tong, S.; Lu, X. Spatiotemporal Change of Aboveground Biomass and Its Response to Climate Change in Marshes of the Tibetan Plateau. *Int. J. Appl. Earth Obs. Geoinf.* **2021**, *102*, 102385. [CrossRef]
57. Damavandi, A.A.; Rahimi, M.; Yazdani, M.R.; Noroozi, A.A. Assessment of Drought Severity Using Vegetation Temperature Condition Index (VTCI) and Terra/MODIS Satellite Data in Rangelands of Markazi Province, Iran. *J. Rangel. Sci.* **2016**, *6*, 33–41.
58. Negret, B.S.; Pérez, F.; Markesteijn, L.; Castillo, M.J.; Armesto, J.J. Diverging Drought-Tolerance Strategies Explain Tree Species Distribution along a Fog-Dependent Moisture Gradient in a Temperate Rain Forest. *Oecologia* **2013**, *173*, 625–635. [CrossRef]
59. Hernández-Stefanoni, J.L.; Castillo-Santiago, M.Á.; Mas, J.F.; Wheeler, C.E.; Andres-Mauricio, J.; Tun-Dzul, F.; George-Chacón, S.P.; Reyes-Palomeque, G.; Castellanos-Basto, B.; Vaca, R.; et al. Improving Aboveground Biomass Maps of Tropical Dry Forests by Integrating LiDAR, ALOS PALSAR, Climate and Field Data. *Carbon Balance Manag.* **2020**, *15*, 15. [CrossRef]
60. de Meira Junior, M.S.; Pinto, J.R.R.; Ramos, N.O.; Miguel, E.P.; de Oliveira Gaspar, R.; Phillips, O.L. The Impact of Long Dry Periods on the Aboveground Biomass in a Tropical Forest: 20 Years of Monitoring. *Carbon Balance Manag.* **2020**, *15*, 12. [CrossRef]
61. Blanco, A.C.; Babaan, J.B.; Escoto, J.E.; Alcantara, C.K. Modelling of Land Surface Temperature Using Gray Level Co-Occurrence Matrix and Random Forest Regression. *Int. Arch. Photogramm. Remote Sens. Spat. Inf. Sci.* **2020**, *XLIII-B3-2020*, 23–28. [CrossRef]
62. Iqbal, N.; Mumtaz, R.; Shafi, U.; Zaidi, S.M.H. Gray Level Co-Occurrence Matrix (GLCM) Texture Based Crop Classification Using Low Altitude Remote Sensing Platforms. *PeerJ Comput. Sci.* **2021**, *7*, e536. [CrossRef]
63. Ciobotaru, A.-M.; Andronache, I.; Ahammer, H.; Radulovic, M.; Peptenatu, D.; Pintilii, R.-D.; Drăghici, C.-C.; Marin, M.; Carboni, D.; Mariotti, G.; et al. Application of Fractal and Gray-Level Co-Occurrence Matrix Indices to Assess the Forest Dynamics in the Curvature Carpathians—Romania. *Sustainability* **2019**, *11*, 6927. [CrossRef]
64. Cairns, M.A.; Brown, S.; Helmer, E.H.; Baumgardner, G.A. Root Biomass Allocation in the World’s Upland Forests. *Oecologia* **1997**, *111*, 1–11. [CrossRef] [PubMed]
65. Gillman, L.N.; Wright, S.D.; Cusens, J.; McBride, P.D.; Malhi, Y.; Whittaker, R.J. Latitude, Productivity and Species Richness. *Glob. Ecol. Biogeogr.* **2015**, *24*, 107–117. [CrossRef]
66. Ullah, F.; Gilani, H.; Sanaei, A.; Hussain, K.; Ali, A. Stand Structure Determines Aboveground Biomass across Temperate Forest Types and Species Mixture along a Local-Scale Elevational Gradient. *For. Ecol. Manag.* **2021**, *486*, 118984. [CrossRef]
67. Zhu, K.; Zhang, J.; Niu, S.; Chu, C.; Luo, Y. Limits to Growth of Forest Biomass Carbon Sink under Climate Change. *Nat. Commun.* **2018**, *9*, 2709. [CrossRef] [PubMed]
68. González-Elizondo, M.S.; González-Elizondo, M.; Tena-Flores, J.A.; Ruacho-González, L.; López-Enríquez, I.L. Vegetación de La Sierra Madre Occidental, México: Una Síntesis. *Acta Bot. Mex.* **2012**, *100*, 351–403. [CrossRef]
69. Ma, W.; Jia, G.; Zhang, A. Multiple Satellite-Based Analysis Reveals Complex Climate Effects of Temperate Forests and Related Energy Budget. *J. Geophys. Res. Atmos.* **2017**, *122*, 3806–3820. [CrossRef]
70. Gibbard, S.; Caldeira, K.; Bala, G.; Phillips, T.J.; Wickett, M. Climate Effects of Global Land Cover Change. *Geophys. Res. Lett.* **2005**, *32*, L23705. [CrossRef]
71. Strilesky, S.L.; Humphreys, E.R. A Comparison of the Net Ecosystem Exchange of Carbon Dioxide and Evapotranspiration for Treed and Open Portions of a Temperate Peatland. *Agric. For. Meteorol.* **2012**, *153*, 45–53. [CrossRef]
72. Liu, L.; Wang, Z.; Wang, Y.; Zhang, Y.; Shen, J.; Qin, D.; Li, S. Trade-off Analyses of Multiple Mountain Ecosystem Services along Elevation, Vegetation Cover and Precipitation Gradients: A Case Study in the Taihang Mountains. *Ecol. Indic.* **2019**, *103*, 94–104. [CrossRef]

73. Galicia, L.; López-Blanco, J.; Zarco-Arista, A.E.; Filips, V.; García-Oliva, F. The Relationship between Solar Radiation Interception and Soil Water Content in a Tropical Deciduous Forest in Mexico. *CATENA* **1999**, *36*, 153–164. [[CrossRef](#)]
74. Wright, D.H. Species-Energy Theory: An Extension of Species-Area Theory. *Oikos* **1983**, *41*, 496. [[CrossRef](#)]

**Disclaimer/Publisher's Note:** The statements, opinions and data contained in all publications are solely those of the individual author(s) and contributor(s) and not of MDPI and/or the editor(s). MDPI and/or the editor(s) disclaim responsibility for any injury to people or property resulting from any ideas, methods, instructions or products referred to in the content.